JOURNAL OF VIROLOGY, Feb. 2008, p. 1748–1758 Vol. 82, No. 4
0022-538X/08/$08.00+0 doi:10.1128/JVI.02014-07

Hippocampal Poly(ADP-Ribose) Polymerase 1 and Caspase 3 Activation in Neonatal Bornavirus Infection▽

Brent L. Williams, Mady Hornig, Kavitha Yaddanapudi, and W. Ian Lipkin*

Center for Infection and Immunity, Mailman School of Public Health of Columbia University, New York, New York

Received 12 September 2007/Accepted 19 November 2007

Infection of neonatal rats with Borna disease virus results in a characteristic behavioral syndrome and apoptosis of subsets of neurons in the hippocampus, cerebellum, and cortex (neonatal Borna disease [NBD]). In the NBD rat hippocampus, dentate gyrus granule cells progressively degenerate. Apoptotic loss of granule cells in NBD is associated with accumulation of zinc in degenerating neurons and reduced zinc in granule cell mossy fibers. Excess zinc can trigger poly(ADP-ribose) polymerase 1 (PARP-1) activation, and PARP-1 activation can mediate neuronal death. Here, we evaluate hippocampal PARP-1 mRNA and protein expression levels, activation, and cleavage, as well as apoptosis-inducing factor (AIF) nuclear translocation and executioner caspase 3 activation, in NBD rats. PARP-1 mRNA and protein levels were increased in NBD hippocampi. PARP-1 expression and activity were increased in granule cell neurons and glia with enhanced ribosylation of proteins, including PARP-1 itself. In contrast, levels of poly(ADP-ribose) glycohydrolase mRNA were decreased in NBD hippocampi. PARP-1 cleavage and AIF expression were also increased in astrocytes in NBD hippocampi. Levels of activated caspase 3 protein were increased in NBD hippocampi and localized to nuclei, mossy fibers, and dendrites of granule cell neurons. These results implicate aberrant zinc homeostasis, PARP-1, and caspase 3 activation as contributing factors in hippocampal neurodegeneration in NBD.

Borna disease virus (BDV) is a nonsegmented, negative-sense, single-stranded RNA virus that persistently infects the central nervous systems (CNS) of and causes behavioral disturbances in a wide range of mammalian and avian species (18, 25). Experimental infection of adult immunocompetent Lewis rats causes a severe meningoencephalitis and a progressive movement disorder that may be associated with detected alterations of the dopamine system and immune-mediated damage (29, 52). In contrast, newborn rats infected with BDV (neonatal borna disease [NBD]) do not mount an overt cellular immune response yet have prominent neuronal loss; pronounced astrogliosis and microgliosis; altered cytokine, neurotrophic factor, and neurotrophic factor receptor gene expression; abnormal development of brain monoaminergic systems; neuronal and astrocytic endoplasmic reticulum (ER) stress; and disturbances of learning, mood, and behavior (11, 31, 38, 45, 62, 67). Although BDV is noncytolytic, NBD is attended by apoptotic degeneration of neurons that undergo substantial postnatal maturation, especially in the hippocampus (HC), cerebellum (CBLM), and cortex (31, 60). Neuronal loss in the CBLM is associated with the induction of ER stress in Purkinje cells, expression of the proapototic molecule C/EBP homologous protein (CHOP), and deficient expression of ER quality control molecules. However, apoptosis of HC dentate gyrus granule cell neurons (DGNs) is not associated with the clear signs of ER disturbances found in other brain regions (62). Thus, the molecular mechanisms contributing to HC neurodegeneration in NBD remain unclear and may be distinct from those in the CBLM.

BDV preferentially infects the limbic system, including the HC, where the highest viral load is consistently reported in NBD rats (10, 25). DGNs in the HC are extensively affected, with continuing apoptotic loss and eventual dissolution of the granule cell layer by postnatal day 45 (PND45) to PND55 (10, 31, 67). In NBD, zinc accumulates in the somata of degenerating DGNs in conjunction with zinc depletion in granule cell mossy fibers, decreased levels of mossy fiber zinc transporter 3 expression, astrocytic induction of metallothioneins, subcellular redistribution of metallothionein III, and sprouting of mossy fibers into the inner molecular layer of the dentate gyrus (61). Neuronal zinc translocation plays a causal role in hippocampal neurodegeneration in seizure, ischemia, brain trauma, and hypoglycemia models (20, 36, 53, 54, 55). However, the mechanism by which excess zinc mediates neuronal death has not been clearly defined. Excess zinc can inhibit key glycolytic enzymes, induce $p75^{NTR}$ and the $p75^{NTR}$-associated death executor, and induce oxidative stress and DNA damage, leading to activation of poly(ADP-ribose) polymerase 1 (PARP-1) (35, 43, 49, 50). Zinc deficiency also induces apoptosis, a process that is at least partially dependent on caspase 3 activation (57). Findings that both excess and deficient zinc culminate in cell death highlight the importance of cellular zinc homeostasis in maintaining cell viability.

Zinc and PARP-1 activation are linked by studies demonstrating PARP-1 activation and cell death following in vitro neuronal exposure to zinc and abrogation of zinc-induced cell death by PARP-1 inhibitors (35, 50, 51, 58). PARP-1 participates in diverse physiological reactions, such as DNA damage repair, transcription, cell death, recombination, regulation of chromosome structure, cell differentiation and proliferation, and microglial activation (33, 48). When activated by DNA damage, PARP-1 consumes NAD^+ to synthesize polymers of ADP-ribose (PAR) onto acceptor proteins, including PARP-1

* Corresponding author. Mailing address: Center for Infection and Immunity, Mailman School of Public Health, Columbia University, 722 West 168th Street, Room 1801, New York, NY 10032. Phone: (212) 342-9033. Fax: (212) 342-9044. E-mail: wil2001@columbia.edu.

▽ Published ahead of print on 5 December 2007.

itself, histones, p53, and DNA topoisomerases (16). While PAR catabolism is an extensive posttranslational modification, it is transient due to the unique PAR-degrading activity of poly(ADP-ribose) glycohydrolase (PARG). Thus, the concerted action of PARP-1 and PARG is critical in maintaining the levels of PAR required for diverse cellular processes (7).

Despite its function in DNA repair, overactivation of PARP-1 may lead to cellular NAD^+ depletion, energy failure, mitochondrial-to-nuclear translocation of apoptosis-inducing factor (AIF), and cell death (2, 13, 65). PARP-1 can also influence neuronal injury by regulating the brain inflammatory response. Microglia are the resident immune cells of the CNS that migrate to the site of neuronal damage, where they secrete cytokines and free radicals that may contribute to CNS injury. Microglial activation and proliferation are dependent on PARP-1 and its interactions with the transcription factor nuclear factor κB (NF-κB) (14, 33).

While a role for PARP-1 activation in neurodegeneration has been described in animal models of excitotoxicity, ischemia, traumatic brain injury, and CNS inflammation (59, 64), few studies have examined the contribution of PARP-1 to viral pathogenesis. PARP-1 ADP-ribosylates simian virus 40 (SV40) large T antigen and is activated by the SV40 minor structural protein VP3, facilitating SV40 release from infected cells; facilitates retroviral integration into the host genome; modifies core proteins of adenovirus; is activated during Sindbis virus infection, leading to cell death; and is involved in polyomavirus VP1 removal from viral DNA, promoting early viral gene expression (4, 12, 19, 21, 24, 27, 39).

In this study, we examine the expression, distribution, activation, and cleavage of PARP-1, as well as AIF expression and caspase 3 activation, in NBD rat brains. Our results implicate enhanced PARP-1 expression and PARP-1 and caspase 3 activation as contributing factors in HC neurodegeneration and the glial response to persistent BDV infection of the CNS.

MATERIALS AND METHODS

Animals and virus inoculation. Lewis rat dams were obtained from Charles River Laboratories (Wilmington, MA). Within 12 h of birth, Lewis rat pups (n = 30) were inoculated in the right cerebral hemisphere with 50 μl of 5×10^3 tissue culture infectious units of BDV strain He/80-1 (NBD) or phosphate-buffered saline (control: sham inoculated). The rats were sacrificed at PND28 for nucleic acid, protein, and anatomic analyses.

RNA extraction. At PND28 postinoculation, NBD (n = 7) and control (n = 5) rats were terminally anesthetized with CO_2. The HC were immediately dissected, snap frozen in TRIzol (Invitrogen, Carlsbad, CA), and stored at −80°C. Following extraction using standard protocols, RNA was quantitated by UV spectrophotometry.

Quantitative Sybr green real-time PCR. Intron/exon-spanning PCR primers specific for rat PARP, PARG, and porphobilinogen deaminase (PBGD) as a housekeeping gene control were designed for real-time PCR using Primer Express 1.0 software (Applied Biosystems, Foster City, CA) (Table 1). PCR standards for determining copy numbers of target transcripts were cloned into the vector pGEM-T easy (Promega Corporation, Madison, WI). Linearized plasmids were quantitated by UV spectroscopy, and 10-fold serial dilutions were created in water containing *Saccharomyces cerevisiae* tRNA (1 ng/μl). RNA from the HC of individual animals was used for real-time PCR assays. cDNA was synthesized using TaqMan reverse transcription reagents (Applied Biosystems) from 2 μg RNA per 100-μl reaction mixture from the HC of each of seven NBD rats and five control rats; each sample was assayed in triplicate. Each 25-μl amplification reaction mixture contained 10 μl template cDNA, 12.5 μl Sybr green master mix (Applied Biosystems), and gene-specific primers at the concentrations indicated in Table 1. The thermal-cycling profile using a Model 7700 sequence detector system (Applied Biosystems) consisted of stage 1, one cycle at 50°C for 2 min; stage 2, 1 cycle at 95°C for 10 min; and stage 3, 45 cycles at 95°C for 15 seconds and 60°C for 1 min. A PBGD fragment was amplified in triplicate reactions by real-time PCR on the same plate as the gene of interest. The mean concentration of PBGD in each sample was used to control for the integrity of input RNA and to normalize the values of target gene expression to those of the housekeeping gene expression. The final results were expressed as the mean number of copies per 200 ng total RNA for PARP and PARG relative to values obtained for PBGD RNA.

TABLE 1. Primers used in this work

Gene (accession no.)	Primer pairs (5′–3′) [reaction concn]	Amplicon size (bp)
PARP-1 (NM_013063)	For: CGCTCAAGGCTCAG AACGAG [100 nM] Rev: CAGGATTGCGGACT CTCCA [100 nM]	130
PARG (AB019366)	For: GTTCCAAAACCGTT TCCAACA [300 nM] Rev: GCAGTTCGCTCACC ATTCTCA [300 nM]	115
PBGD (X06827)	For: ATTCGGGGAAACCT CAACACC [300 nM] Rev: CTGACCCACAGCAT ACATGCAT [300 nM]	157

Western blot analysis. Individual HC were dissected from PND28 NBD (n = 4) and control (n = 4) rats and homogenized in ice-cold hypotonic cell lysis buffer (20 mM HEPES, pH 7.9, 400 mM NaCl, 1 mM EDTA, 1 mM EGTA, and 1 mM dithiothreitol) containing protease inhibitors (Complete Mini EDTA-free tablets; Roche Molecular Biochemicals, Indianapolis, IN) and incubated on ice for 30 min. The homogenates were centrifuged at 15,000 × g for 20 min at 4°C. The supernatants containing proteins were collected, and the protein concentrations were estimated by Bradford assay (Bio-Rad, Hercules, CA). Protein lysates (30 μg) in sample buffer (10 mM Tris-HCl, pH 7.5, 10 mM EDTA, 20% [vol/vol] glycerol, 1% [wt/vol] sodium dodecyl sulfate, 0.005% [wt/vol] bromophenol blue, 100 mM dithiothreitol, 1% [vol/vol] beta-mercaptoethanol) were boiled for 5 min and size fractionated by 10% sodium dodecyl sulfate-polyacrylamide gel electrophoresis. The proteins were transferred to nitrocellulose membranes using a semidry blotting apparatus (Owl Separation Systems, Portsmouth, NH). The membranes were blocked in 2% nonfat milk powder in 20 mM Tris-HCl, pH 7.6, 137 mM NaCl, 0.1% Tween 20 (TTBS) overnight at room temperature and incubated with rabbit anti-PARP antibody (Ab) (1:200; H-250; Santa Cruz Biotechnology), mouse anti-PAR monoclonal Ab (MAb) (1:400; 10H; Alexis Biochemicals, San Diego, CA), or rabbit anti-cleaved caspase 3 Ab (1:500; Asp175; Cell Signaling Technology, Danvers, MA), in TTBS with 1% nonfat milk for 2 h at room temperature. The membranes were washed three times for 10 min each time with TTBS prior to incubation with peroxidase-conjugated goat anti-mouse immunoglobulin G (IgG) (1:2,000; Bio-Rad) or goat anti-rabbit IgG (1:2,000; Bio-Rad) in TTBS with 1% nonfat dry milk for 1 h at room temperature. The membranes were developed using the ECL Western blot detection system (Amersham Biosciences, Arlington Heights, IL) and scanned for chemiluminescence using a Storm 840 imager (Molecular Dynamics, Sunnyvale, CA). The blots were stripped and reprobed with mouse anti-GAPDH (glyceraldehyde-3-phosphate dehydrogenase) MAb (Ambion, Austin, TX), as a housekeeping gene and for loading control and normalization. Protein bands were quantitated using Image Quant software (v.1.0; Molecular Dynamics).

TUNEL. Cellular-DNA fragmentation was labeled in brain sections by terminal deoxynucleotidyltransferase (TdT)-mediated dUTP-biotin nick end labeling (TUNEL), using diaminobenzidine as a chromogen (22). Cryostat sections were fixed in 4% paraformaldehyde and treated with 1 μg/ml proteinase K (Roche, Indianapolis, IN) for 5 min at 37°C. The sections were washed with phosphate-buffered saline (PBS), fixed in paraformaldehyde, treated with 0.3% hydrogen peroxide in 0.1 M phosphate buffer for 20 min, and dehydrated through graded ethanol solutions. The sections were covered with a mixture of 1 mM biotinylated 16-dUTP (Roche), 10 mM dATP (Roche), TdT enzyme (Promega, Madison, WI), 5× TdT buffer (Promega), and distilled H_2O and incubated at 37°C for 1 h. After the sections were washed in PBS, visualization of the reaction was carried out using a Vectastain Elite ABC kit (Vector Laboratories, Burlingame, CA) and

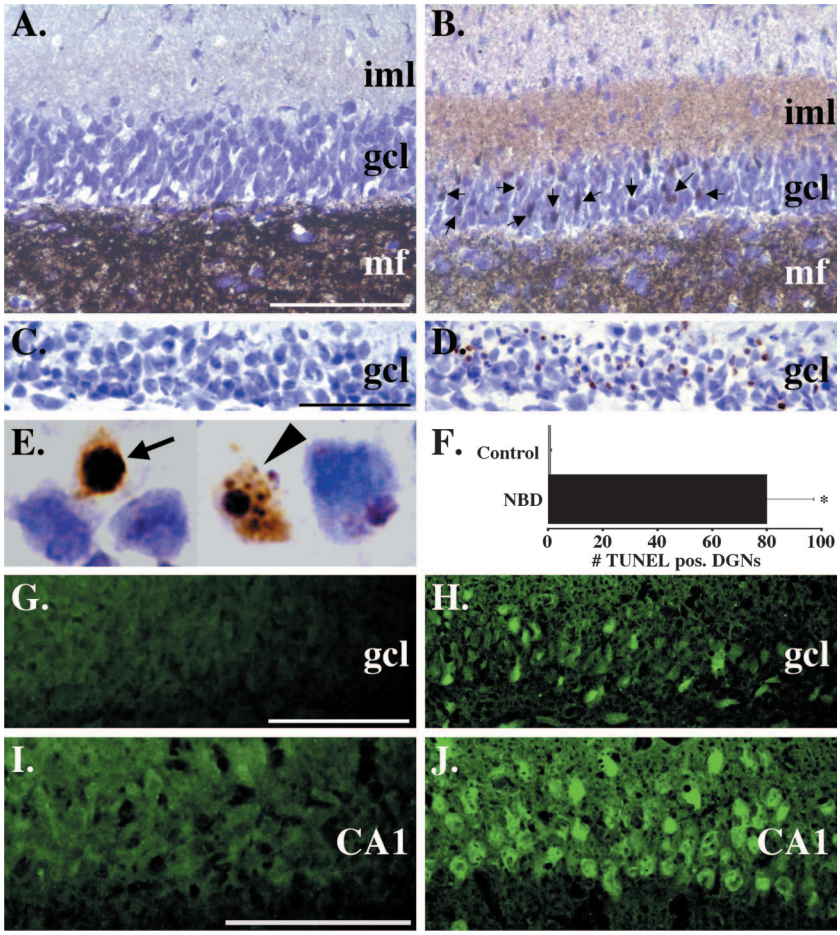

FIG. 1. Granule cell degeneration, zinc distribution, and apoptosis in the NBD HC. (A) Timm's staining (dark-brown stain) in PND28 control rat dentate gyrus. gcl, granule cell layer; iml, inner molecular layer; mf, mossy fibers. (B) Timm's staining in PND28 NBD rat dentate gyrus; note the accumulation of zinc in DGNs (arrows), decreased intensity of zinc stain in mossy fibers, and increased intensity of zinc stain in the iml. (C) Representative TUNEL of PND28 control rat DGNs. (D) Representative TUNEL of PND28 NBD rat DGNs; note the numerous TUNEL-positive neurons (brown stain). (E) TUNEL-positive DGNs with pyknotic nuclei (arrow) and signs of nuclear fragmentation (arrowhead). (F) Quantitation of TUNEL-positive DGNs in control ($n = 4$; 0.75 ± 0.479 cells) and PND28 NBD ($n = 4$; 80 ± 17.213 cells) rats (ANOVA, $P = 0.0037$). The data are presented as the mean number of DGNs per dentate gyrus $\pm$ standard error of the mean. The asterisk indicates a P value of <0.05. (G and H) IF staining for BDV nucleoprotein in control (G) and NBD (H) rat DGNs. (I and J) IF staining for BDV nucleoprotein in control (I) and NBD (J) rat hippocampal CA1 region pyramidal neurons. Bars = 100 μm.

diaminobenzidine as a substrate (Vector Laboratories) according to the manufacturer's instructions. The slides were counterstained with hematoxylin, mounted, and visualized with a light microscope at ×100 magnification. For counting of TUNEL-positive neurons, approximately 700 granule cells per dentate gyrus from the dorsal and ventral blades, as well as the dorsal-ventral junction, were analyzed for each PND28 control ($n = 4$) and NBD ($n = 4$) rat at ×100 magnification. Cells with intense brown nuclear staining or brown staining of fragmented DNA within the cell were scored as TUNEL positive.

Histological and IF analyses. Under CO_2 anesthesia, PND28 NBD ($n = 4$) and control ($n = 4$) rats were perfused via left ventricular puncture with PBS (1 ml/g body weight), followed by buffered 4% paraformaldehyde (1 ml/g body weight). Their brains were postfixed in 4% paraformaldehyde overnight at 4°C and cryoprotected with graded sucrose solutions. Cryostat sections (14 μm) were collected onto glass slides (Super Frost Plus; Fisher Scientific, Pittsburgh, PA). Timm's staining and immunofluorescence (IF) microscopy were carried out as previously described (61). The following primary Abs were used for IF: rabbit anti-BDV N protein (1:1,500) (62), rabbit anti-PARP Ab (1:50; H-250; Santa Cruz Biotechnology), mouse anti-PAR MAb (1:50; 10H; Alexis Biochemicals), rabbit anti-PARP p85 fragment Ab (1:50; Promega Corporation, Madison, WI), rabbit anti-cleaved caspase 3 Ab (1:50; Asp175; Cell Signaling Technology), rabbit anti-glial fibrillary acidic protein (GFAP) Ab (1:200; Dako Cytomation, Carpinteria, CA), mouse anti-GFAP MAb cocktail (1:30; BD Pharmingen, San Diego, CA), mouse anti-neuronal nuclei (NeuN) MAb (1:100; Chemicon International, Temecula, CA), mouse OX-42 MAb (1:100; Chemicon), rabbit anti-Iba1 Ab (2 μg/ml; Wako Pure Chemicals Industries, Ltd., Richmond, VA), rabbit anti-AIF (1:50; Chemicon), and goat anti-AIF (1:30; D-20; Santa Cruz Biotechnology). Secondary Abs were Cy3-conjugated anti-mouse, anti-rabbit, or anti-goat IgG (1:200; Jackson Immunoresearch Laboratories, Inc., West Grove, PA) and/or Cy2-conjugated anti-mouse or anti-rabbit IgG (1:200; Jackson Immunoresearch).

Statistical analysis. The significance of observed differences between NBD and control groups was assessed by analysis of variance (ANOVA) for TUNEL-positive cell counts, real-time PCR, and Western immunoblot analysis. Analysis was carried out using StatView software (v.5.0.1; SAS Institute Inc., Cary, NC). Values were considered to be significant when P was <0.05.

RESULTS

Dentate gyrus granule cell neurodegeneration: zinc and apoptosis. Progressive apoptotic loss of DGNs is a hallmark of NBD. Consistent with our previous report, Timm's staining for zinc (a dark-brown reaction product) was normal in control

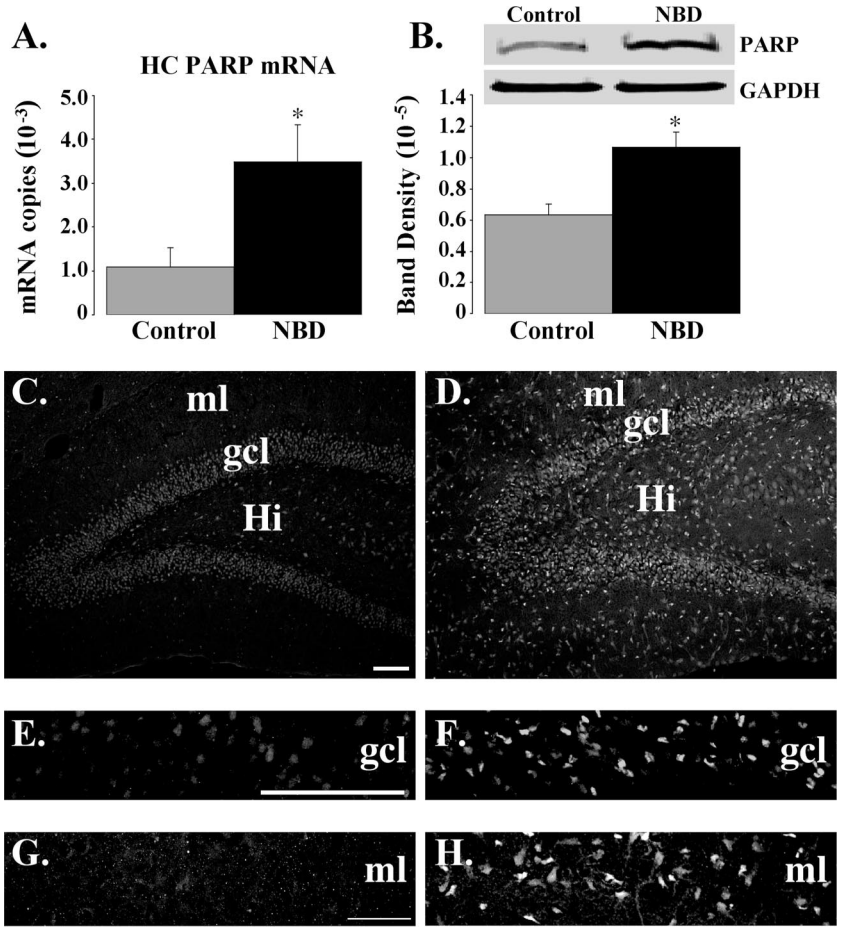

FIG. 2. PARP-1 mRNA and protein expression in NBD and control rat brains. (A) Real-time PCR analysis of PARP-1 mRNA in HC of PND28 control ($n = 5$) and NBD ($n = 7$) rats. PARP-1 mRNA in HC was significantly increased for NBD relative to control rats (3.18-fold increase in NBD; ANOVA, $P = 0.044$). The asterisk indicates a P value of <0.05. The error bars indicate standard errors of the means (SEM). (B) Representative Western immunoblots for PARP-1 protein (top) in extracts from control or NBD rat HC. Corresponding immunoblot signals for GAPDH are shown (bottom). The bar graph shows the determination of the PARP-1 protein band density relative to the GAPDH signal in extracts from control ($n = 4$) or NBD ($n = 4$) rat HC. HC PARP-1 protein levels were significantly increased in extracts from NBD rats relative to controls (1.68-fold increase in NBD; ANOVA, $P = 0.012$). PARP-1 IF in control (C, E, and G) and NBD (D, F, and H) rat HC. Note the faint staining of DGNs in control rats (C and E) and increased staining of DGNs in NBD rats (D and F). Few PARP-1-positive cells were apparent in the molecular layers of control rats (C and G) compared to numerous PARP-1-positive cells scattered throughout the molecular layers of NBD rats (D and H). gcl, granule cell layer; ml, molecular layer; Hi, hilus. Bars = 100 μm.

rats (Fig. 1A; note the prominent Timm's stain in the mossy fibers). In PND28 NBD rats, zinc accumulated in the somata of DGNs (Fig. 1B) and was associated with increased Timm's staining in the inner molecular layer and decreased Timm's staining in the mossy fibers (Fig. 1B) (61). TUNEL in HC of individual control rats revealed few, if any, TUNEL-positive DGNs (Fig. 1C). In contrast, numerous TUNEL-positive DGNs were present in PND28 NBD rats (Fig. 1D). TUNEL-labeled DGNs in NBD rats had apoptotic morphology consistent with the morphology of degenerating DGNs harboring zinc in their somata (61), including nuclear pyknosis (Fig. 1E) and nuclear/chromatin fragmentation (Fig. 1E). Quantitation of TUNEL-positive DGNs in control and NBD rat HC revealed rare TUNEL-positive DGNs in control rats (0.75 ± 0.479 cells/dentate gyrus), while approximately 10% of all DGNs were TUNEL positive in NBD rats (80 ± 17.213 cells/dentate gyrus) (Fig. 1F). Whereas immunostaining revealed only scattered infected DGNs (Fig. 1G and H), nearly all pyramidal neurons of CA1 harbored BDV antigen (Fig. 1I and J).

PARP-1 mRNA and protein expression in PND28 NBD rats. Although PARP-1 protein has been shown to colocalize with zinc-laden DGNs in NBD rats (61), PARP-1 expression has not been quantitated. Sybr green real-time PCR demonstrated increases in PARP-1 mRNA in PND28 NBD HC relative to control rat HC (Fig. 2A) (3.18-fold; ANOVA, $P = 0.044$). The increase in PARP-1 mRNA was correlated with increased PARP-1 protein levels. Protein extracts from control and NBD HC were analyzed by Western blotting. PARP-specific Abs detected a single band of 116 kDa corresponding to the expected size of PARP-1 in both control and NBD HC extracts (Fig. 2B). Quantitation of PARP-1 band densities normalized to GAPDH (housekeeping control) revealed increased PARP-1 protein levels in NBD HC

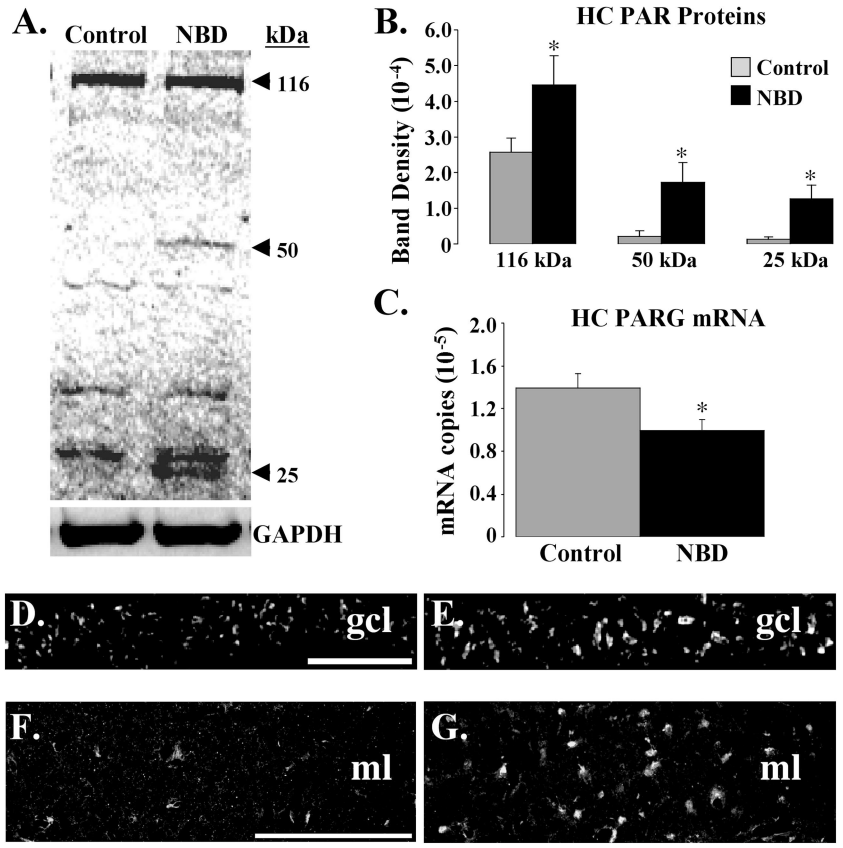

FIG. 3. Enhanced poly(ADP-ribosyl)ation of proteins in NBD rats. (A) Protein lysates from HC of PND28 control ($n = 4$) and NBD ($n = 4$) rats were evaluated by Western analysis using Abs specific for PAR. (B) Determination of protein band densities relative to that for GAPDH revealed increased ribosylation of PARP-1 (116 kDa; 1.74-fold increase; ANOVA, $P = 0.05$), an unknown 50-kDa protein (8.25-fold increase; ANOVA, $P = 0.02$), and an unknown 25-kDa protein (9.15-fold increase; ANOVA, $P = 0.03$). The asterisks indicate P values of <0.05. The error bars indicate SEM. (C) Real-time PCR analysis of PARG mRNA in HC of PND28 control ($n = 5$) or NBD ($n = 7$) rats. PARG mRNA was significantly decreased for NBD rats relative to the results for control rats (1.4-fold decrease; ANOVA, $P = 0.041$). (D to G) IF analysis for PAR in DGNs (D and E) and the dentate molecular layer (F and G) of PND28 control (D and F) and NBD (E and G) rats. Note the enhanced IF in DGNs and cells in the molecular layer of NBD relative to control rats. gcl, granule cell layer; ml, molecular layer. Bars = 100 μm.

relative to control rats (1.68-fold; ANOVA, $P = 0.012$) (Fig. 2B).

HC expression of PARP-1 was assessed in brain sections of PND28 control and NBD rats by IF microscopy. In control rats, the PARP-1 signal was weak in cells of the HC (Fig. 2C). In NBD rats, the PARP-1 signal was increased in scattered cells throughout the HC (Fig. 2D). DGNs stained faintly for PARP-1 in control rats (Fig. 2E). In NBD, numerous DGNs were strongly immunoreactive for PARP-1 (Fig. 2F). Few glial cells in the molecular layer of the dentate gyrus of control rats were immunoreactive for PARP-1 (Fig. 2G). In NBD rats, the density of PARP-1 immunoreactive glial cells in the molecular layer was increased relative to control rats (Fig. 2H).

PARP-1 activation in HC. PARP-1 catalyzes the addition of long chains of PAR onto target proteins, including itself, using NAD^+ as the substrate. In order to assess the ribosylation status of specific proteins in the HC of NBD rats, we analyzed HC protein lysates from control and NBD rats by Western immunoblotting using Abs to PAR and GAPDH (loading control) (Fig. 3A). In both control and NBD rats, the major band that was recognized by the PAR antibody was 116 kDa, consistent with the mass of PARP-1. Additional 50-kDa and 25-kDa bands were present in NBD rat lysates. Individual band densities were quantitated and normalized to GAPDH. This analysis revealed significant increases in the 116-kDa (representing PARP-1) (1.74-fold; ANOVA, $P = 0.05$), the 50-kDa (8.25-fold; ANOVA, $P = 0.02$), and the 25-kDa (9.15-fold; ANOVA, $P = 0.03$) species in NBD relative to control rats (Fig. 3B).

Homeostatic control of poly(ADP-ribosyl)ation is regulated by the enzyme PARG, which rapidly hydrolyzes PAR units into free ADP-ribose. To assess whether altered PARG expression could contribute to increased PAR levels, we evaluated PARG mRNA levels in the HC of PND28 control and NBD rats. Sybr green real-time PCR revealed a significant decrease in PARG mRNA in NBD rats relative to controls (1.4-fold; ANOVA, $P = 0.041$) (Fig. 3C).

IF analysis revealed moderate PAR staining in control rat HC, especially in DGNs (Fig. 3D). The intensity of the PAR signal was increased in numerous DGNs of PND28 NBD rats (Fig. 3E). The density of PAR-stained glial cells in the molecular layer of the dentate gyrus of control rats (Fig. 3F) was lower than in NBD rats (Fig. 3G).

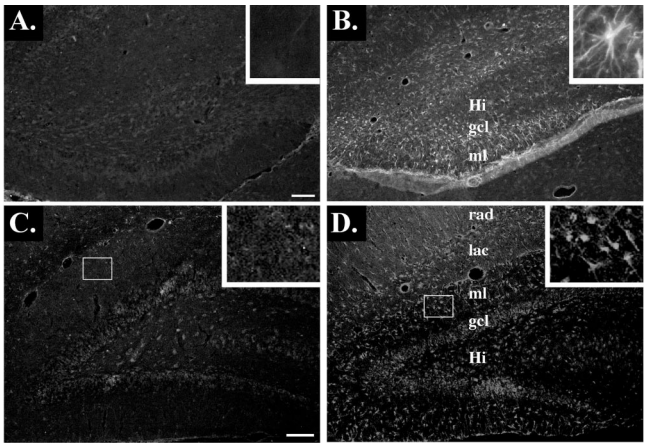

FIG. 4. Cleavage of PARP-1 and AIF expression in NBD rat glia. (A and B) IF analysis with p85PARP-1 Abs in PND28 control (A) and NBD (B) rat HC. Note the increased IF for p85PARP-1 in astrocytes (colocalization with GFAP is not shown) throughout the molecular layer of the dentate gyrus of NBD rats. (B, inset) Higher magnification of a p85PARP-1 immunoreactive astrocyte. (C and D) IF analysis with AIF Abs in PND28 control (C) and NBD (D) rat HC. Note the increased expression of AIF in astrocytes in the NBD rat HC (D, inset). gcl, granule cell layer; ml, molecular layer; Hi, hilus; lac, stratum lacunosum-moleculare; rad, stratum radiatum. Bars = 100 μm.

PARP-1 cleavage and AIF expression in astrocytes. Cleavage of PARP-1 is commonly used as an indicator of apoptosis. Therefore, we analyzed PARP-1 cleavage in the HC by IF analysis using an antibody specific to the p85 cleavage product of PARP-1 (p85PARP-1). IF for p85PARP-1 was weak in control rat HC (Fig. 4A). In contrast, strong p85PARP-1 IF was detected in the HC of NBD rats, especially in the dentate gyrus (Fig. 4B). Higher magnification revealed strong staining in glial cells (Fig. 4B, inset). IF colocalization of p85PARP-1 and GFAP confirmed that p85PARP-1-positive cells were astrocytes (data not shown).

Overactivation of PARP-1 is required for mitochondrial release of AIF. Given our findings of increased expression and activation of PARP-1 in NBD rat brain neurons and glia, we evaluated the potential contribution of AIF as a downstream mediator of neurodegeneration in NBD. IF analysis of AIF in PND28 control (Fig. 4C) and NBD (Fig. 4D) rat HC did not reveal nuclear translocation of AIF in NBD DGNs; however, AIF expression was enhanced in glial cells throughout the molecular layer of the dentate gyrus, stratum lacunosum moleculare, and stratum radiatum (Fig. 4D, inset). Double-label IF studies using anti-GFAP revealed that AIF-positive cells were astrocytes (data not shown).

Caspase 3 activation in NBD rat HC. The observation that zinc accumulation and PARP-1 overexpression and activation in the NBD HC were not associated with caspase-independent AIF translocation led us to examine whether caspase-dependent cell death mechanisms might contribute to DGN demise. Caspase 3 acts as a key downstream executioner of apoptosis (3, 34, 37). Activation of caspase 3 requires cleavage of the inactive 32-kDa proenzyme (40). To determine whether caspase 3 is activated in the HC of NBD rats, protein extracts from NBD and control rat HC were evaluated by Western blotting using an antibody specific for the cleaved fragments of caspase 3. The 17-kDa and 19-kDa cleaved forms of caspase 3 were visible in all NBD protein extracts, but not in control rat extracts (Fig. 5A, immunoblot). Quantitation of band densities for cleaved caspase 3 revealed significant increases in NBD relative to control extracts for regions in the immunoblot corresponding to the 17-kDa (14.4-fold; ANOVA, $P = 0.01$) and 19-kDa (6.83-fold; ANOVA, $P = 0.008$) species (Fig. 5A, bar graph).

IF analysis of activated caspase 3 in control rat HC revealed only weak staining of DGNs in the inner granule cell layer (Fig. 5B and D) and a few astrocytes in the molecular layer of the dentate gyrus (Fig. 5B and F). IF analysis of NBD rat HC indicated strong staining of activated caspase 3 in DGNs (Fig. 5C and E) and numerous astrocytes in the molecular layer (Fig. 5C and G).

In NBD rats, increased levels of activated caspase 3 were clearly observed in DGN mossy fibers and dendrites. Activated caspase 3 IF was not observed in control rat mossy fibers (Fig. 5H), while strong staining was apparent in NBD rat mossy fibers (Fig. 5I). In addition, activated caspase 3-positive DGN dendrites extending into the molecular layer of the dentate gyrus were observed only in NBD rats (Fig. 5J).

Colocalization of PARP-1, PAR, AIF, and caspase 3 with cellular markers. The cellular distribution of increased PARP-1 expression and activation was assessed by double-label IF in NBD HC using Abs to PARP-1 and anti-PAR, anti-NeuN (neuronal marker), anti-OX42 (microglial marker), or anti-GFAP (astrocytic marker). PARP-1 expression in the dentate gyrus granule cell layer (Fig. 2) was confirmed to represent expression in DGNs. A representative DGN double labeled for PARP-1 and NeuN is shown in Fig. 6A. PAR signal also colocalized with DGNs that overexpressed PARP-1 (Fig. 6B). While PAR signal was detected in most infected DGNs (Fig. 6C), many DGNs had strong PAR signal in the absence of BDV antigen (Fig. 6C). Many cells with strong PARP-1 signal in the molecular layer of the dentate gyrus colocalized with the microglial marker OX42 (Fig. 6D). Although the signal was weaker than that observed for microglia, enhanced PARP-1 expression was also evident in GFAP-positive astrocytes in the molecular layer (Fig. 6E; the boxed cell shows stronger staining in the microglia). These results confirm that PARP-1 expression and activity are increased in DGNs, microglia, and astrocytes.

Double-label IF was also used to confirm cellular localization of activated caspase 3. While activated caspase 3 was predominately localized in intact nuclei of NeuN-positive DGNs, in some cells, activated caspase 3 was also present in the cytoplasm surrounding multifragmented nuclei (Fig. 6F). Activated caspase 3 was also observed in NeuN-positive neurons in the cortex (Fig. 6G and 7A) and GFAP-positive astrocytes in the cortex (Fig. 6G) and HC (Fig. 6H).

PARP-1, PAR, and caspase 3 in the cortex and CBLM. Neurodegeneration in NBD is not restricted to the HC. IF analysis was carried out using Abs to PARP-1, PAR, and activated caspase 3 in the cortices (Fig. 7A) and CBLM (Fig. 7B) of control and NBD rats in order to evaluate their contributions in other affected brain regions. PARP-1 IF was not increased in cortical neurons in NBD rats compared to controls (Fig. 7A); however, NBD cortical microglia stained strongly for PARP-1 (Fig. 7A). Cortical neuronal PAR IF levels were also

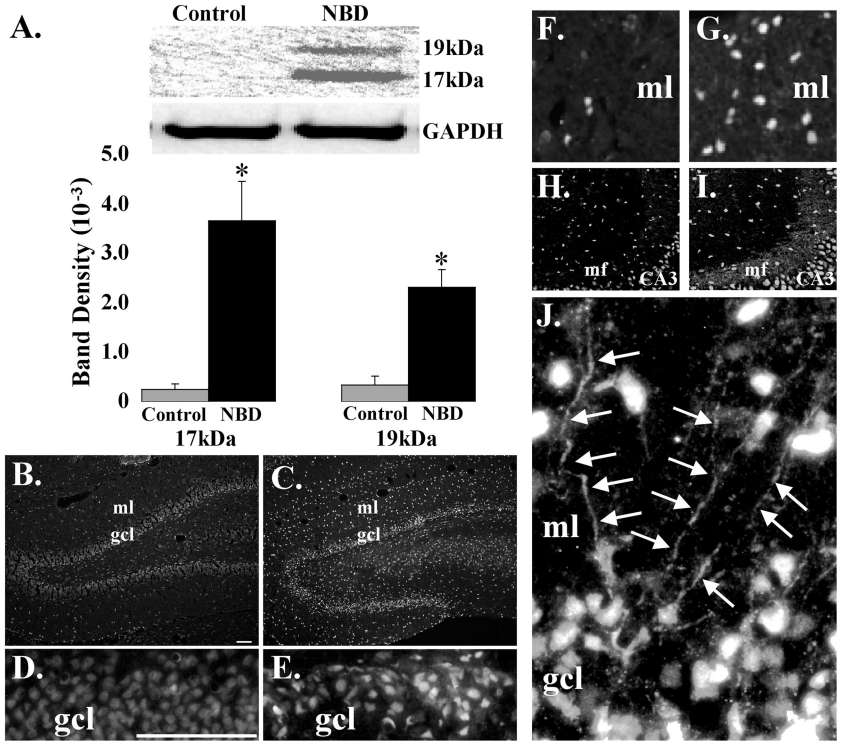

FIG. 5. Caspase 3 activation in the NBD rat HC. (A) Protein lysates from the HC of PND28 control and NBD rats were evaluated by Western analysis using Abs specific for activated (cleaved) caspase 3. Note that activated caspase 3 was not detected in any lysates from control rats but was present as strong bands in all NBD lysates. The bar graph shows the determination of protein band densities from control ($n = 4$) and NBD ($n = 4$) protein extracts, which revealed significantly increased levels for both the 17-kDa (14.4-fold increase; ANOVA, $P = 0.01$) and 19-kDa (6.83-fold increase; ANOVA, $P = 0.008$) species of activated caspase 3 in NBD HC relative to corresponding blot regions of control rat lysates. The asterisks indicate P values of <0.05. The error bars indicate SEM. (B to J) IF analysis of activated caspase 3 in the HC of control (B, D, F, and H) and NBD (C, E, G, I, and J) rats. (D and E) Higher-magnification views of DGNs in control (D) and NBD (E) rats. (F and G) Activated caspase 3 immunopositive astrocytes in the dentate molecular layer of control (F) and NBD (G) rats. (H to J) Immunolocalization of activated caspase 3 in axons and dendrites of NBD DGNs. Shown is activated caspase 3 IF in control (H) and NBD (I) rat DGN mossy fibers and NBD DGN dendrites extending into the molecular layer of the dentate gyrus (J, arrows). gcl, granule cell layer; ml, molecular layer; CA3, stratum pyramidale of the CA3 subregion. Bars = 100 μm.

similar in control and NBD rats (Fig. 7A). In contrast, activated caspase 3 IF was increased in some cortical neurons of NBD rats compared to controls (Fig. 7A).

PARP-1 and PAR IF signals were similar in control and NBD CBLM (Fig. 7B). Activated caspase 3 showed similar distributions in Bergmann glia lining the Purkinje layer and astrocytes in the granule cell layer of control and NBD rats (Fig. 7B). No activated caspase 3 was detected in Purkinje neurons of control or NBD rats.

DISCUSSION

Neonatal viral infections are important causes of neurodevelopmental damage; however, the molecular mechanisms by which damage can be mediated are poorly understood. In NBD, degeneration of DGNs is associated with zinc accumulation in the somata of neurons and loss of zinc from their axons (61). Altered zinc homeostasis may initiate a cascade of molecular events culminating in neuronal cell loss. Here, we report enhanced expression and activation of PARP-1 and caspase 3 activation in NBD rat DGNs. In addition, our findings of enhanced glial PARP-1 expression, activation, and cleavage, as well as enhanced AIF expression, suggest an important role for these molecules in the inflammatory response to neonatal infection in the brain.

Zinc translocation into neurons can induce oxidative stress, DNA damage, and PARP-1 activation (35). PARP-1 plays a role in cellular damage in various disease models, including stroke, trauma, ischemia, arthritis, β-cell cytotoxicity, 1-methyl-4phenyl-1,2,3,6-tetrahydropyridine exposure, experimental autoimmune encephalomyelitis, hypoglycemia, and endotoxic shock (59, 64). Overactivation of PARP-1 and catabolism of PAR polymers onto cellular proteins consumes NAD^+, depleting cellular energy stores and leading to cell death. Additionally, PAR polymer is directly toxic to neurons and can induce mitochondrial AIF release, translocation to the nucleus, and cell death (2, 65). Here, we report that zinc translocation into DGN somata occurs in conjunction with increased PARP-1 mRNA and protein expression in the HC. Enhanced catabolism of PAR on proteins (including PARP-1 itself) and enhanced immunostaining for PAR in NBD DGNs demonstrate PARP-1 activation in these vulnerable HC neurons. Additionally, we found decreased mRNA levels for the main PAR-degrading enzyme, PARG, in the NBD HC. These results demonstrate that PARP-1 activity is increased in the NBD HC and may be directly related to increased levels of PARP-1

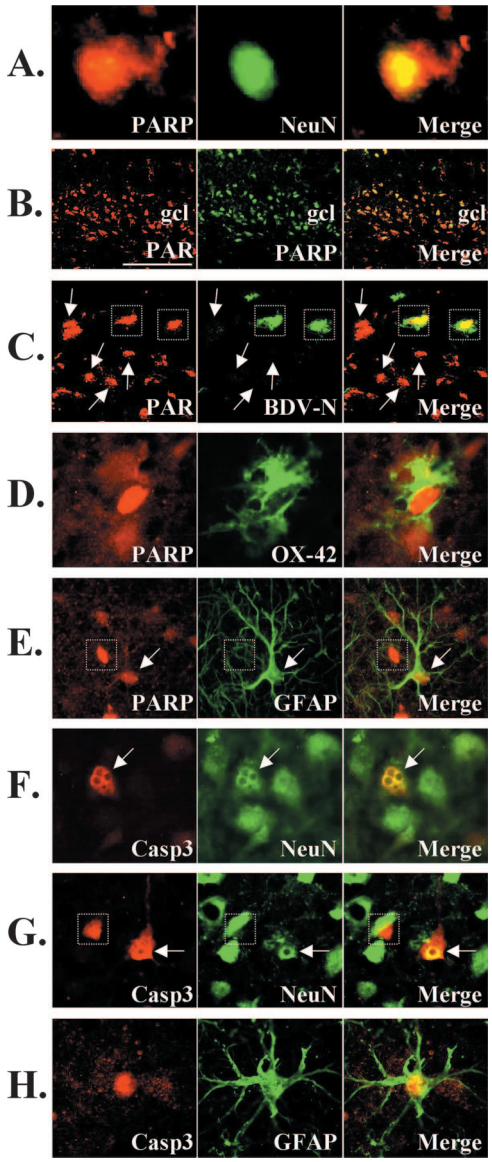

FIG. 6. Colocalization of molecular markers. (A) Double-label IF showing colocalization of PARP-1 and the neuronal marker NeuN in PND28 NBD rat DGNs. (B) Double-label IF showing colocalization of PAR and PARP in PND28 NBD rat DGNs. (C) Double-label IF showing colocalization of PAR and BDV N in PND28 NBD rat DGNs (boxed cells). Note that many DGNs have strong PAR signal in the absence of viral antigen (arrows). (D) Double-label IF showing colocalization of PARP-1 and the microglial marker OX-42 in the molecular layer of the HC of a PND28 NBD rat. (E) Double-label IF showing colocalization of PARP-1 and the astrocytic marker GFAP (arrow indicates double-labeled astrocyte) in PND28 NBD rat HC; note the stronger PARP-1 staining in microglia (boxed cell). (F) Double-label IF showing colocalization of activated caspase 3 and NeuN in DGN of a PND28 NBD rat (arrow indicates double-labeled DGN). (G) Double-label IF showing colocalization of activated caspase 3 and NeuN in a cortical neuron (arrow indicates double-labeled cortical neuron) of a PND28 NBD rat; note the caspase 3-positive astrocyte in the cortex (boxed cell). (H) Double-label IF showing colocalization of activated caspase 3 and GFAP in the molecular layer of the dentate gyrus of a PND28 NBD rat.

expression and/or deficient PARG-mediated hydrolysis of PAR. Interestingly, DGN infection by BDV does not appear to be a prerequisite for PARP-1 activation. Although increased ribosylation of proteins was detected in DGNs harboring viral antigen, many PAR-positive DGNs lacked detectable viral protein. Discordance between direct viral infection and PARP-1 activation in DGNs suggests that, at least in part, indirect factors contribute to activation of PARP-1 and DGN damage.

The mitochondrial flavoprotein AIF is released from the mitochondria, translocates to the nucleus, and contributes to neurodegeneration in brain trauma, brain ischemia, and mouse models of amyotrophic lateral sclerosis and in response to hydrogen peroxide, peroxynitrite, p53 overexpression, *N*-methyl-D-aspartate, and 1-methyl-4 phenylpyridinium (8, 9, 15, 41, 66). We did not detect nuclear AIF translocation in DGNs of NBD rats, despite enhanced PARP-1 expression and activation. However, we cannot exclude the possibility that low levels of AIF, below the level of detection, contribute to apoptosis in NBD.

In NBD, PARP-1 activity may play a direct role in apoptosis through PARP-1 overexpression and overactivation in DGNs. However, PARP-1 and PAR expression was also found in HC microglia and astrocytes. A prominent role for glial cell activation in the pathophysiology of CNS diseases and neurotoxicity has been extensively documented (23, 32). Glial cell activation results in synthesis of inflammatory mediators, such as reactive radicals (i.e., nitric oxide and superoxide anion) and cytokines (i.e., interleukin-1β [IL-1β], IL-6, and tumor necrosis factor alpha), that mediate the apoptotic and excitotoxic deaths of neurons (1, 5, 17). PARP-1 plays a key role in regulating NF-κB-driven transcription of proinflammatory cytokines (28, 42). During lipopolysaccharide plus gamma interferon- or Aβ1-40-induced glial activation, PARP-1 activity promotes DNA binding by NF-κB. Pharmacological inhibition of PARP-1 inhibits glial activation, reduces NF-κB activity, inhibits the production of inflammatory mediators, and reduces associated neurotoxicity (14). Increased levels of proinflammatory cytokines (i.e., IL-1β, IL-1α, IL-6, and tumor necrosis factor alpha) in NBD brains have been reported by several groups (11, 31). Thus, enhanced PARP-1 activity in glial cells may indirectly mediate neuronal death in NBD by promoting glial production and release of inflammatory mediators.

Although infected astrocytes do not undergo apoptotic elimination in NBD (10), PARP-1 protein expression, activation, and cleavage and enhanced AIF protein expression may hint at underlying dysfunction. Persistently infected astrocytes have impaired glutamate uptake and express classic markers of ER stress (6, 62). Excess zinc inhibits astrocytic glutamate uptake; this effect is dependent on PARP-1 activation (56). Thus, zinc released from mossy fibers may play a dual role in DGN injury by directly injuring neurons and indirectly by inhibiting astrocyte-mediated protection from glutamate toxicity.

Zinc deficiency may also be neurotoxic. Zinc deficiency-induced apoptosis is dependent on caspase 3 activation (57). Activated caspase 3 has been reported in axons (including mossy fibers) and dendrites in the HC following ischemia, when zinc levels are decreased in mossy fibers (36, 46). In NBD, we found increased levels of activated caspase 3 in nuclei, mossy fibers, and dendrites of DGNs in association with decreased levels of zinc in mossy fibers. Thus, zinc deficiency in mossy fibers could contribute to enhanced activation of caspase 3 and subsequent apoptosis of DGNs.

PARP-1 cleavage is a hallmark of apoptosis; however, its

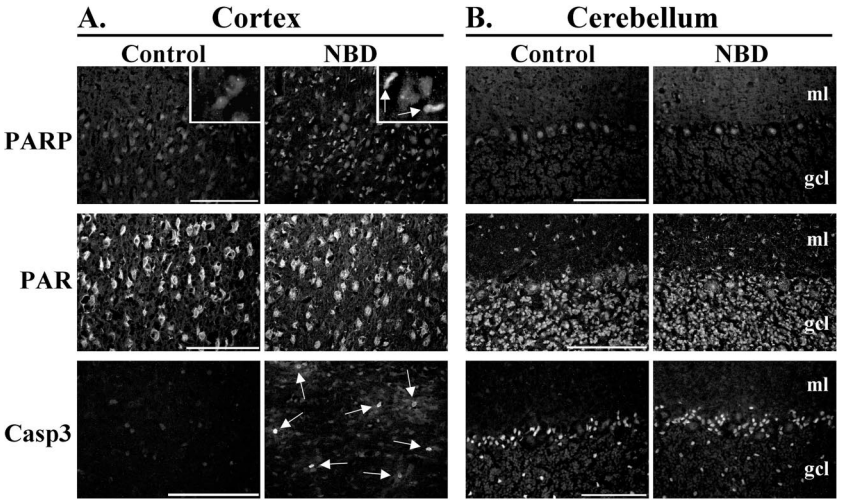

FIG. 7. PARP-1, PAR, and activated caspase 3 in cortex and CBLM. (A) IF analysis of PARP-1 (top row; arrows indicate PARP-1 immunoreactive microglia), PAR (middle row), and activated caspase 3 (bottom row; arrows indicate activated caspase 3-positive cortical neurons) in the cortices of PND28 control (left) and NBD (right) rats. (B) IF analysis of PARP-1 (top row), PAR (middle row), and activated caspase 3 (bottom row) in the CBLM of PND28 control (left) and NBD (right) rats.

role in the phenomenon is unclear. Cleavage of PARP-1 may inactivate the DNA repair system, prevent PARP-mediated NAD^+ and ATP depletion, and deribosylate endonucleases implicated in DNA fragmentation. During apoptosis, activated caspase 3 cleaves PARP-1, inhibiting its catalytic activity. Fibroblasts engineered to express cleavage-resistant PARP-1 are more susceptible to apoptotic stimuli (30). In cell-free systems, zinc inhibits PARP-1 cleavage by caspase 3 (44). High levels of zinc in DGN somata in NBD may inhibit caspase 3-mediated cleavage of PARP-1, facilitating the apoptotic process in DGNs by maintaining PARP-1 in its active state. As noted above, astrocytes in NBD have not been reported to undergo apoptosis. Astrocytes in NBD HC were caspase 3 positive and expressed both PARP-1 and the p85PARP-1 cleavage product. We speculate that PARP-1 cleavage in astrocytes could contribute to their survival in NBD by preventing overactivation and depletion of energy stores.

Neuronal vulnerability and mechanisms of neurodegeneration may be regionally discordant during viral infections of the CNS. Factors that may contribute to the differential effects of viral infections on neuronal subtypes include variability in the kinetics of viral replication in neural subpopulations, the maturational status of neurons, differential expression of cellular survival/death genes between neuronal populations, and regionally distinct levels of excitotoxins and expression of their receptors on neurons. Both caspase 3-dependent and -independent mechanisms contribute regionally to neuronal death following West Nile virus infection in mice (47). Distinct death mechanisms are activated by Sindbis virus infection, depending on the neuronal subtype and maturation status of infected neurons (26). Maturation status and selective expression of molecular markers (e.g., aldolase C and excitatory amino acid transporter 4) appear to be important determinants regulating patterns of Purkinje cell death in NBD (63). Interestingly, whereas Purkinje cells and cortical neurons express ER stress markers, DGNs do not (62). Conversely, whereas DGNs accumulate zinc and have enhanced PARP-1 expression and activity, cortical and Purkinje neurons do not (61). The high physiological concentration of zinc in DGN mossy fibers may be a vital determinant in the susceptibility of DGNs to cell death in NBD. Although further study is warranted, evidence is emerging to suggest that different neuronal populations may undergo cell-specific death programs in response to neonatal infection.

ACKNOWLEDGMENTS

This work was supported by NIH awards NS29425 and HD37546.

REFERENCES

1. **Allan, S. M., and N. J. Rothwell.** 2001. Cytokines and acute neurodegeneration. Nat. Rev. Neurosci. **2:**734–744.
2. **Andrabi, S. A., N. S. Kim, S. W. Yu, H. Wang, D. W. Koh, M. Sasaki, J. A. Klaus, T. Otsuka, Z. Zhang, R. C. Koehler, P. D. Hurn, G. G. Poirier, V. L. Dawson, and T. M. Dawson.** 2006. Poly(ADP-ribose) (PAR) polymer is a death signal. Proc. Natl. Acad. Sci. USA **103:**18308–18313.
3. **Armstrong, R. C., T. J. Aja, K. D. Hoang, S. Gaur, X. Bai, E. S. Alnemri, G. Litwack, D. S. Karanewsky, L. C. Fritz, and K. J. Tomaselli.** 1997. Activation of the CED3/ICE-related protease CPP32 in cerebellar granule neurons undergoing apoptosis but not necrosis. J. Neurosci. **17:**553–562.
4. **Baksi, K., H. Alkhatib, and M. E. Smulson.** 1987. In vivo characterization of the poly(ADP-ribosylation) of SV40 chromatin and large T antigen by immunofractionation. Exp. Cell Res. **172:**110–123.
5. **Bezzi, P., M. Domercq, L. Brambilla, R. Galli, D. Schols, E. De Clercq, A. Vescovi, G. Bagetta, G. Kollias, J. Meldolesi, and A. Volterra.** 2001. CXCR4-activated astrocyte glutamate release via TNFα: amplification by microglia triggers neurotoxicity. Nat. Neurosci. **4:**702–710.
6. **Billaud, J. N., C. Ly, T. R. Phillips, and J. C. de la Torre.** 2000. Borna disease virus persistence causes inhibition of glutamate uptake by feline primary cortical astrocytes. J. Virol. **74:**10438–10446.
7. **Bonicalzi, M. E., J. F. Haince, A. Droit, and G. G. Poirier.** 2005. Regulation of poly(ADP-ribose) metabolism by poly(ADP-ribose) glycohydrolase: where and when? Cell Mol. Life Sci. **62:**739–750.
8. **Cande, C., F. Cecconi, P. Dessen, and G. Kroemer.** 2002. Apoptosis-inducing factor (AIF): key to the conserved caspase-independent pathways of cell death? J. Cell Sci. **115:**4727–4734.
9. **Cao, G., R. S. Clark, W. Pei, W. Yin, F. Zhang, F. Y. Sun, S. H. Graham, and J. Chen.** 2003. Translocation of apoptosis-inducing factor in vulnerable neurons after transient cerebral ischemia and in neuronal cultures after oxygen-glucose deprivation. J. Cereb. Blood Flow Metab. **23:**1137–1150.
10. **Carbone, K. M., T. R. Moench, and W. I. Lipkin.** 1991. Borna disease virus replicates in astrocytes, Schwann cells and ependymal cells in persistently infected rats: location of viral genomic and messenger RNAs by in situ hybridization. J. Neuropathol. Exp. Neurol. **50:**205–214.
11. **Carbone, K. M., S. A. Rubin, Y. Nishino, and M. V. Pletnikov.** 2001. Borna

disease: virus-induced neurobehavioral disease pathogenesis. Curr. Opin. Microbiol. **4:**467–475.
12. **Carbone, M., A. Reale, A. Di Sauro, O. Sthandier, M. I. Garcia, R. Maione, P. Caiafa, and P. Amati.** 2006. PARP-1 interaction with VP1 capsid protein regulates polyomavirus early gene expression. J. Mol. Biol. **363:**773–785.
13. **Chiarugi, A.** 2002. Poly(ADP-ribose) polymerase: killer or conspirator? The 'suicide hypothesis' revisited. Trends Pharmacol. Sci. **23:**122–129.
14. **Chiarugi, A., and M. A. Moskowitz.** 2003. Poly(ADP-ribose) polymerase-1 activity promotes NF-κB-driven transcription and microglial activation: implication for neurodegenerative disorders. J. Neurochem. **85:**306–317.
15. **Chu, C. T., J. H. Zhu, G. Cao, A. Signore, S. Wang, and J. Chen.** 2005. Apoptosis inducing factor mediates caspase-independent 1-methyl-4-phenylpyridinium toxicity in dopaminergic cells. J. Neurochem. **94:**1685–1695.
16. **D'Amours, D., S. Desnoyers, I. D'Silva, and G. G. Poirier.** 1999. Poly(ADP-ribosyl)ation reactions in the regulation of nuclear functions. Biochem. J. **342:**249–268.
17. **Dawson, V. L., and T. M. Dawson.** 1998. Nitric oxide in neurodegeneration. Prog. Brain Res. **118:**215–229.
18. **de la Torre, J. C.** 1994. Molecular biology of Borna disease virus: prototype of a new group of animal viruses. J. Virol. **68:**7669–7675.
19. **Dery, C. V., G. de Murcia, D. Lamarre, N. Morin, G. G. Poirier, and J. Weber.** 1986. Possible role of ADP-ribosylation of adenovirus core proteins in virus infection. Virus Res. **4:**313–329.
20. **Frederickson, C. J., M. D. Hernandez, S. A. Goik, J. D. Morton, and J. F. McGinty.** 1988. Loss of zinc staining from hippocampal mossy fibers during kainic acid induced seizures: a histofluorescence study. Brain Res. **446:**383–386.
21. **Gaken, J. A., M. Tavassoli, S. U. Gan, S. Vallian, I. Giddings, D. C. Darling, J. Galea-Lauri, M. G. Thomas, H. Abedi, V. Schreiber, J. Menissier-de Murcia, M. K. Collins, S. Shall, and F. Farzaneh.** 1996. Efficient retroviral infection of mammalian cells is blocked by inhibition of poly(ADP-ribose) polymerase activity. J. Virol. **70:**3992–4000.
22. **Gavrieli, Y., Y. Sherman, and S. A. Ben-Sasson.** 1992. Identification of programmed cell death in situ via specific labeling of nuclear DNA fragmentation. J. Cell Biol. **119:**493–501.
23. **González-Scarano, F., and G. Baltuch.** 1999. Microglia as mediators of inflammatory and degenerative diseases. Annu. Rev. Neurosci. **22:**219–240.
24. **Gordon-Shaag, A., Y. Yosef, M. Abd El-Latif, and A. Oppenheim.** 2003. The abundant nuclear enzyme PARP participates in the life cycle of simian virus 40 and is stimulated by minor capsid protein VP3. J. Virol. **77:**4273–4282.
25. **Gosztonyi, G., and H. Ludwig.** 1995. Borna disease—neuropathology and pathogenesis. Curr. Top. Microbiol. Immunol. **190:**39–73.
26. **Griffin, D. E.** 2005. Neuronal cell death in alphavirus encephalomyelitis. Curr. Top. Microbiol. Immunol. **289:**57–77.
27. **Ha, H. C., K. Juluri, Y. Zhou, S. Leung, M. Hermankova, and S. H. Snyder.** 2001. Poly(ADP-ribose) polymerase-1 is required for efficient HIV-1 integration. Proc. Natl. Acad. Sci. USA **98:**3364–3368.
28. **Ha, H. C., L. D. Hester, and S. H. Snyder.** 2002. Poly(ADP-ribose) polymerase-1 dependence of stress-induced transcription factors and associated gene expression in glia. Proc. Natl. Acad. Sci. USA **99:**3270–3275.
29. **Hatalski, C. G., W. F. Hickey, and W. I. Lipkin.** 1998. Evolution of the immune response in the central nervous system following infection with Borna disease virus. J. Neuroimmunol. **90:**137–142.
30. **Herceg, Z., and Z. Q. Wang.** 1999. Failure of poly(ADP-ribose) polymerase cleavage by caspases leads to induction of necrosis and enhanced apoptosis. Mol. Cell. Biol. **19:**5124–5133.
31. **Hornig, M., H. Weissenbock, N. Horscroft, and W. I. Lipkin.** 1999. An infection-based model of neurodevelopmental damage. Proc. Natl. Acad. Sci. USA **96:**12102–12107.
32. **Iadecola, C., and M. Alexander.** 2001. Cerebral ischemia and inflammation. Curr. Opin. Neurol. **14:**89–94.
33. **Kauppinen, T. M., and R. A. Swanson.** 2005. Poly(ADP-ribose) polymerase-1 promotes microglial activation, proliferation, and matrix metalloproteinase-9-mediated neuron death. J. Immunol. **174:**2288–2296.
34. **Keane, R. W., A. Srinivasan, L. M. Foster, M. P. Testa, T. Ord, D. Nonner, H. G. Wang, J. C. Reed, D. E. Bredesen, and C. Kayalar.** 1997. Activation of CPP32 during apoptosis of neurons and astrocytes. J. Neurosci. Res. **48:**168–180.
35. **Kim, Y. H., and J. Y. Koh.** 2002. The role of NADPH oxidase and neuronal nitric oxide synthase in zinc-induced poly(ADP-ribose) polymerase activation and cell death in cortical culture. Exp. Neurol. **177:**407–418.
36. **Koh, J. Y., S. W. Suh, B. J. Gwag, Y. Y. He, C. Y. Hsu, and D. W. Choi.** 1996. The role of zinc in selective neuronal death after transient global cerebral ischemia. Science **272:**1013–1016.
37. **Kuida, K., T. S. Zheng, S. Na, C. Kuan, D. Yang, H. Karasuyama, P. Rakic, and R. A. Flavell.** 1996. Decreased apoptosis in the brain and premature lethality in CPP32-deficient mice. Nature **384:**368–372.
38. **Narayan, O., S. Herzog, K. Frese, H. Scheefers, and R. Rott.** 1983. Behavioral disease in rats caused by immunopathological responses to persistent Borna virus in the brain. Science **220:**1401–1403.
39. **Nargi-Aizenman, J. L., C. M. Simbulan-Rosenthal, T. A. Kelly, M. E. Smulson, and D. E. Griffin.** 2002. Rapid activation of poly(ADP-ribose) polymerase contributes to Sindbis virus and staurosporine-induced apoptotic cell death. Virology **293:**164–171.
40. **Nicholson, D. W., A. Ali, N. A. Thornberry, J. P. Vaillancourt, C. K. Ding, M. Gallant, Y. Gareau, P. R. Griffin, M. Labelle, Y. A. Lazebnik, N. A. Munday, S. M. Raju, M. E. Smulson, T. Yamin, V. L. Yu, and D. K. Miller.** 1995. Identification and inhibition of the ICE/CED-3 protease necessary for mammalian apoptosis. Nature **376:**17–18.
41. **Oh, Y. K., K. S. Shin, and S. J. Kang.** 2006. AIF translocates to the nucleus in the spinal motor neurons in a mouse model of ALS. Neurosci. Lett. **406:**205–210.
42. **Oliver, F. J., J. Ménissier-de Murcia, C. Nacci, P. Decker, R. Andriantsitohaina, S. Muller, G. de la Rubia, J. C. Stoclet, and G. de Murcia.** 1999. Resistance to endotoxic shock as a consequence of defective NF-κB activation in poly(ADP-ribose) polymerase-1 deficient mice. EMBO J. **18:**4446–4454.
43. **Park, J. A., J. Y. Lee, T. A. Sato, and J. Y. Koh.** 2000. Co-induction of p75NTR and p75NTR-associated death executor in neurons after zinc exposure in cortical culture or transient ischemia in the rat. J. Neurosci. **20:**9096–9103.
44. **Perry, D. K., M. J. Smyth, H. R. Stennicke, G. S. Salvesen, P. Duriez, G. G. Poirier, and Y. A. Hannun.** 1997. Zinc is a potent inhibitor of the apoptotic protease, caspase-3. A novel target for zinc in the inhibition of apoptosis. J. Biol. Chem. **272:**18530–18533.
45. **Pletnikov, M. V., S. A. Rubin, G. J. Schwartz, K. M. Carbone, and T. H. Moran.** 2000. Effects of neonatal rat Borna disease virus (BDV) infection on the postnatal development of the brain monoaminergic systems. Brain Res. Dev. Brain Res. **119:**179–185.
46. **Rami, A., S. Jansen, I. Giesser, and J. Winckler.** 2003. Post-ischemic activation of caspase-3 in the rat hippocampus: evidence of an axonal and dendritic localisation. Neurochem. Int. **43:**211–223.
47. **Samuel, M. A., J. D. Morrey, and M. S. Diamond.** 2007. Caspase 3-dependent cell death of neurons contributes to the pathogenesis of West Nile virus encephalitis. J. Virol. **81:**2614–2623.
48. **Schreiber, V., F. Dantzer, J. C. Ame, and G. de Murcia.** 2006. Poly(ADP-ribose): novel functions for an old molecule. Nat. Rev. Mol. Cell Biol. **7:**517–528.
49. **Sensi, S. L., H. Z. Yin, S. G. Carriedo, S. S. Rao, and J. H. Weiss.** 1999. Preferential Zn^{2+} influx through Ca^{2+}-permeable AMPA/kainate channels triggers prolonged mitochondrial superoxide production. Proc. Natl. Acad. Sci. USA **96:**2414–2419.
50. **Sheline, C. T., M. M. Behrens, and D. W. Choi.** 2000. Zinc-induced cortical neuronal death: contribution of energy failure attributable to loss of NAD^+ and inhibition of glycolysis. J. Neurosci. **20:**3139–3146.
51. **Sheline, C. T., H. Wang, A. L. Cai, V. L. Dawson, and D. W. Choi.** 2003. Involvement of poly ADP ribosyl polymerase-1 in acute but not chronic zinc toxicity. Eur. J. Neurosci. **18:**1402–1409.
52. **Solbrig, M. V., G. F. Koob, J. N. Joyce, and W. I. Lipkin.** 1996. A neural substrate of hyperactivity in Borna disease: changes in brain dopamine receptors. Virology **222:**332–338.
53. **Suh, S. W., J. W. Chen, M. Motamedi, B. Bell, K. Listiak, N. F. Pons, G. Danscher, and C. J. Frederickson.** 2000. Evidence that synaptically-released zinc contributes to neuronal injury after traumatic brain injury. Brain Res. **852:**268–273.
54. **Suh, S. W., R. B. Thompson, and C. J. Frederickson.** 2001. Loss of vesicular zinc and appearance of perikaryal zinc after seizures induced by pilocarpine. Neuroreport **12:**1523–1525.
55. **Suh, S. W., P. Garnier, K. Aoyama, Y. Chen, and R. A. Swanson.** 2004. Zinc release contributes to hypoglycemia-induced neuronal death. Neurobiol. Dis. **16:**538–545.
56. **Suh, S. W., K. Aoyama, C. C. Alano, C. M. Anderson, A. M. Hamby, and R. A. Swanson.** 2007. Zinc inhibits astrocyte glutamate uptake by activation of poly(ADP-ribose) polymerase-1. Mol. Med. **13:**344–349.
57. **Truong-Tran, A. Q., J. Carter, R. E. Ruffin, and P. D. Zalewski.** 2001. The role of zinc in caspase activation and apoptotic cell death. Biometals **14:**315–330.
58. **Virag, L., and C. Szabo.** 1999. Inhibition of poly(ADP-ribose) synthetase (PARS) and protection against peroxynitrite-induced cytotoxicity by zinc chelation. Br. J. Pharmacol. **126:**769–777.
59. **Virag, L., and C. Szabo.** 2002. The therapeutic potential of poly(ADP-ribose) polymerase inhibitors. Pharmacol. Rev. **54:**375–429.
60. **Weissenbock, H., M. Hornig, W. F. Hickey, and W. I. Lipkin.** 2000. Microglial activation and neuronal apoptosis in Bornavirus infected neonatal Lewis rats. Brain Pathol. **10:**260–272.
61. **Williams, B. L., K. Yaddanapudi, C. M. Kirk, A. Soman, M. Hornig, and W. I. Lipkin.** 2006. Metallothioneins and zinc dysregulation contribute to neurodevelopmental damage in a model of perinatal viral infection. Brain Pathol. **16:**1–14.
62. **Williams, B. L., and W. I. Lipkin.** 2006. Endoplasmic reticulum stress and

neurodegeneration in rats neonatally infected with Borna disease virus. J. Virol. **80:**8613–8626.
63. **Williams, B. L., K. Yaddanapudi, M. Hornig, and W. I. Lipkin.** 2007. Spatiotemporal analysis of Purkinje cell degeneration relative to parasagittal expression domains in a model of neonatal viral infection. J. Virol. **81:**2675–2687.
64. **Yu, S. W., H. Wang, T. M. Dawson, and V. L. Dawson.** 2003. Poly(ADP-ribose) polymerase-1 and apoptosis inducing factor in neurotoxicity. Neurobiol. Dis. **14:**303–317.
65. **Yu, S. W., S. A. Andrabi, H. Wang, N. S. Kim, G. G. Poirier, T. M. Dawson, and V. L. Dawson.** 2006. Apoptosis-inducing factor mediates poly(ADP-ribose) (PAR) polymer-induced cell death. Proc. Natl. Acad. Sci. USA **103:**18314–18319.
66. **Zhang, X., J. Chen, S. H. Graham, L. Du, P. M. Kochanek, R. Draviam, F. Guo, P. D. Nathaniel, C. Szabo, S. C. Watkins, and R. S. Clark.** 2002. Intranuclear localization of apoptosis-inducing factor (AIF) and large scale DNA fragmentation after traumatic brain injury in rats and in neuronal cultures exposed to peroxynitrite. J. Neurochem. **82:**181–191.
67. **Zocher, M., S. Czub, J. Schulte-Monting, J. C. de La Torre, and C. Sauder.** 2000. Alterations in neurotrophin and neurotrophin receptor gene expression patterns in the rat CNS following perinatal Borna disease virus infection. J. Neurovirol. **6:**462–477.